Heliyon 9 (2023) e22429

Contents lists available at ScienceDirect

Heliyon

journal homepage: www.cell.com/heliyon

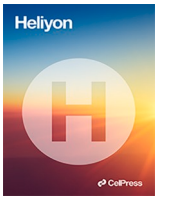

Identification of molecular subtypes and a risk model based on inflammation-related genes in patients with low grade glioma

Cheng Long [a], Ya Song [a], Yimin Pan [b,**], Changwu Wu [b,c,*]

[a] Department of Orthopedics, Xiangya Hospital, Central South University, Changsha, 410008, China
[b] Department of Neurosurgery, Xiangya Hospital, Central South University, Changsha, 410008, China
[c] National Clinical Research Center for Geriatric Disorders, Xiangya Hospital, Central South University, Changsha, 410008, China

ARTICLE INFO

Keywords:
Low grade glioma
Risk model
Inflammation
Immune infiltration
Prognosis
Molecular subtyping

ABSTRACT

Lower grade gliomas (LGGs) exhibit invasiveness and heterogeneity as distinguishing features. The outcome of patients with LGG differs greatly. Recently, more and more studies have suggested that infiltrating inflammation cells and inflammation-related genes (IRGs) play an essential role in tumorigenesis, prognosis, and treatment responses. Nevertheless, the role of IRGs in LGG remains unclear. In The Cancer Genome Atlas (TCGA) cohort, we conducted a thorough examination of the predictive significance of IRGs and identified 245 IRGs that correlated with the clinical prognosis of individuals diagnosed with LGG. Based on unsupervised cluster analysis, we identified two inflammation-associated molecular clusters, which presented different tumor immune microenvironments, tumorigenesis scores, and tumor stemness indices. Furthermore, a prognostic risk model including ten prognostic IRGs (*ADRB2*, *CD274*, *CXCL12*, *IL12B*, *NFE2L2*, *PRF1*, *SFTPC*, *TBX21*, *TNFRSF11B*, and *TTR*) was constructed. The survival analysis indicated that the IRGs risk model independently predicted the prognosis of patients with LGG, which was validated in an independent LGG cohort. Moreover, the risk model significantly correlated with the infiltrative level of immune cells, tumor mutation burden, expression of HLA and immune checkpoint genes, tumorigenesis scores, and tumor stemness indices in LGG. Additionally, we found that our risk model could predict the chemotherapy response of some drugs in patients with LGG. This study may enhance the advancement of personalized therapy and improve outcomes of LGG.

1. Introduction

Lower grade gliomas (LGG), with invasive and heterogeneous characteristics, are comprised of World Health Organization (WHO) grade I-III gliomas [1]. The majority of patients diagnosed with LGG experience a more gradual progression and comparatively more favorable outcome in comparison to those with (GBM). Currently, treatment for LGG includes clinical observation, neurosurgical resection followed by chemotherapy, and/or radiotherapy. However, LGG remains incurable and cannot be completely resected, and

* Corresponding author. Department of Neurosurgery, Xiangya Hospital, Central South University, 87 Xiangya Road, Changsha, Hunan, 410008, China.
** Corresponding author. Department of Neurosurgery, Xiangya Hospital, Central South University, 87 Xiangya Road, Changsha, Hunan, 410008, China.
E-mail addresses: yimin.pan@foxmail.com (Y. Pan), wuchangwu@csu.edu.cn (C. Wu).

https://doi.org/10.1016/j.heliyon.2023.e22429
Received 10 May 2023; Received in revised form 7 November 2023; Accepted 13 November 2023
Available online 17 November 2023

the residual tumor will reoccur or progress to GBM in most cases [2,3]. Because of the considerable heterogeneity of LGG, the outcome of patients with LGG varies greatly. Studies have increasingly demonstrated that patients with LGG with similar histology and grade differ wildly in terms of prognosis [4]. Although WHO has established several molecular markers, such as IDH1 mutation, 1p/19q codeletion, and H3K27 M mutation, for LGG classification, none of them can comprehensively explain the heterogeneity of LGG. Moreover, individually planning an optimal treatment strategy for LGG remains a challenge, and there has been little progress in enhancing the outcome for patients with LGG in the past decades [5,6]. Therefore, the identification of a novel classification system and molecular targets to develop effective therapeutic strategies and to predict the treatment response for LGG is urgently required.

The tumor microenvironment (TME) is an important component of tumor tissues. The components of TME are complex and include various non-tumor cells, such as tumor-associated macrophages, tumor-infiltrating lymphocytes, natural killer cells, dendritic cells, and extracellular matrix. Recently, many studies have demonstrated that TME participates in multiple processes of cancers, such as initiation and progression of tumors, cell proliferation and differentiation, therapeutic resistance, and immune escape [7,8]. TME is highly plastic and inflammation greatly influences the makeup of TME [9]. The initial inflammatory reaction serves as the primary defense mechanism against external infections and facilitates both innate and adaptive immune responses. Nevertheless, in the event that the prompt resolution of the acute inflammatory reaction does not occur, it could progress into persistent inflammation, resulting in the abundance of immune-suppressive cells (M2 macrophages, Treg cells, MDSC, etc.) and immune-suppressive microenvironment [10–12]. These changes can promote the activation of oncogenes, affect various tumor-related pathways, and facilitate tumor occurrence and growth. In addition, lactic acid in the chronically inflamed microenvironment can promote immune evasion by impacting immune cells such as cytotoxic T cells [13]. Chronic inflammation often accompanies the recruitment of cancer-associated fibroblasts, which are accountable for depositing collagen proteins and diverse components of the extracellular matrix. It has been shown that these fibroblasts can promote cancer cell proliferation and angiogenesis [14,15]. Therefore, chronic inflammation is also a hallmark of cancer, accounting for approximately 25 % of carcinogenic factors [9]. While chronic inflammation has the potential to cause tumor development, it is widely recognized that the majority of inflammatory cells possess the ability to eliminate pathogens and impede the growth of tumors [16]. Cancer immune surveillance, a vital process in preventing cancer, involves the identification and elimination of recently developed tumor cells by the immune system [10]. Numerous studies have shown that certain categories of immune cells, molecules that carry out a specific function, and pathways can occasionally collaborate as natural tumor inhibitors [17]. For example, inflammatory dendritic cells are a subset of dendritic cells that only respond to inflammatory stimuli and are crucial for anti-tumor immune responses [18]. Overall, inflammation is an attractive target for cancer prevention and therapy because the genome of cells that regulate inflammation is relatively stable and these cells do not rapidly develop drug resistance [12]. Nevertheless, the role of inflammation in LGG is still unclear. Therefore, it is particularly important to comprehensively understand inflammation and highlight its underlying mechanism in LGG, which finally is helpful in finding novel markers for LGG and enhance the prognosis of LGG. The use of inflammation-related genes (IRGs) to construct the clinical risk prediction model could also be promising in LGG.

Through extensive analysis in the current study, we identified prognostic IRGs and inflammation-associated molecular subtypes in LGG, and developed a risk model for prognostic prediction through big data mining (Supplementary Fig. S1). In addition, we analyzed the survival stratification, somatic mutations, infiltration level of immune cells, and prediction of chemotherapy response based on the risk characteristics.

2. Material and methods

2.1. Obtaining data

The data, including RNA sequence expression, phenotype, and gene mutation data, of the TCGA-LGG dataset was downloaded from the UCSC Xena (https://xenabrowser.net/). The mRNA expression and clinical data of GSE16011 were downloaded from the Gene Expression Omnibus (GEO, https://www.ncbi.nlm.nih.gov/gds). The TCGA-LGG cohort was used as the training set and the GSE16011 LGG cohort was used as the validation set. The clinical information of all LGG samples included in this study is summarized in Supplementary Table S1. Single-cell RNA sequencing (scRNA-seq) data (GSE102130) was downloaded from GEO database [19]. Then R package “Seurat” and “ggplot2” was used for the data normalization and visualization [20–24]. In total, 4058 cells were extracted from the original dataset for the downstream analysis. After standardized normalization procedures in Seurat, t-distributed stochastic neighbor embedding (t-SNE) was performed to find cell clusters with distinct transcriptomic expression patterns. CD14, CX3CR1, and AIF1 were applied as the markers for the annotation of immune cells, while MAG, MBP, and PLP1 were for oligodendrocytes. The remaining clusters which can be primarily grouped by tumor’s origin were regarded as malignant cells [19]. The expression of related genes was visualized by “DotPlot” and “FeaturePlot” using “Seurat” and “ggplot2”.

2.2. Identification of prognostic IRGs in LGG

We gained the IRGs from the GeneCards database (https://www.genecards.org) and filtered them by the following criteria: protein coding gene and relevance scores >5. We screened out 394 IRGs, and 372 of these IRGs were matched in the TCGA dataset (Supplementary Table S2). To identify prognostic IRGs in LGG, the analysis of univariate Cox was conducted.

2.3. Identification of potential molecular clusters

The 245 prognostic IRGs were used to identify potential inflammation-related molecular subtypes in LGG. We utilized the

"ConsensusClusterPlus" R package to conduct the cluster analysis, with the parameters set according to our previous description [25].

2.4. Development and validation of the prognostic signature

The risk model, which was based on 245 prognosis IRGs, was constructed using the TCGA dataset. First, we combined the clinical data with the expression matrix of 245 prognostic IRGs. Then, the least absolute shrinkage and selection operator (LASSO) regression analysis was performed by using the R packages "glmne" and "survival" [26]. Through the LASSO regression dimensionality reduction, we selected 25 key prognostic IRGs. Subsequently, the expression matrix and clinical data of these 25 IRGs were input into multivariate Cox regression analysis. Finally, 10 significant IRGs were selected in the multivariate Cox regression to develop a risk model, and the coefficients of each IRG in the risk model were also determined through multivariate Cox analysis. The IGRs signature score can be calculated using the following formula: Risk score = −0.22604 * ADRB2 + 0.46830 * CD274–0.79819 * CXCL12 + 0.35033 * IL12B + 0.89678 * NFE2L2 - 0.28079 * PRF1 + 0.15592 * SFTPC +0.52431 * TBX21 + 0.39677 * TNFRSF11B + 0.26237 * TTR. Then, we calculated the risk score of all samples and divided patients with LGG into two groups based on the median value of the risk score. Subsequently, the performance of this risk model was assessed by survival analysis and time-dependent ROC curves. The GSE16011 dataset was used to validate the performance of this risk model by calculating the risk score of all samples. To further validate the robustness of the IGRs signature, we first conducted a univariate Cox analysis to independently analyze the model. Then, we performed multivariable Cox analysis using age, gender, staging, histological subtype, and IDH1 status as covariates to verify if the IGRs signature is an independent risk factor. Additionally, we stratified the patients based on different ages, gender, grade, histological subtypes, and IDH1 status to further analyze the prognosis and determine the efficacy of the risk model in different subgroups.

2.5. Enrichment analysis

To assess the pathways and biological processes enrichment of the high- and low-risk group, the Gene Set Enrichment Analysis (GSEA) was performed by using the "clusterProfiler" package. The Gene Oncology (GO), Kyoto Encyclopedia of Genes and Genomes (KEGG), and HALLMARK gene sets were downloaded from the MSigDB. The criteria for filtering significant terms included adjusted *p-value* < 0.05, as well as absolute normalized enrichment score (NES) > 1. The ssGSEA was performed to calculate four tumorigenesis scores of LGG samples, including mesenchymal-EMT score, angiogenic activity score, tumorigenic cytokines score, and stemness score, by using the "GSAV" package. The gene sets of these tumorigenesis scores were obtained from a previous study [27]. In addition, the single sample GSEA (ssGSEA) was also employed to assess the enrichment level of immune cells in LGG.

2.6. Analysis of immune cell infiltration

Three algorithms were employed to evaluate the enrichment of immune cells. The ssGSEA algorithm estimated 28 immune cells that infiltrated the LGG samples. The TIMER was used to estimate the infiltration level of six immune cells in LGG samples. Furthermore, the ESTIMATE algorithm was employed to compute four TME-associated metrics, namely the ImmuneScore, StromalScore, ESTIMATEScore, and tumor purity for every LGG sample.

2.7. Tumor mutation burden (TMB) and tumor stemness indices (TSIs) analysis

Recently, many studies have suggested that TMB and TSIs are related to the therapeutic response of immune checkpoint inhibitors and might have the ability to predict the efficacy of immunotherapy [28]. The TMB of LGG samples in the TCGA database was calculated by using the R package "maftools". The TSIs were obtained from a previous study [29]. Then, the differential analysis was conducted to assess TMB and TSIs between the subgroups.

2.8. Chemotherapy response analysis

In recent, a methodology has been described to predict the response of drugs, and an R package, called "pRRophetic" has been developed [30]. As we described previously, we used this package to predict the response of drugs of patients and get the IC50 value of drugs of patients based on the data of Genomics of Drug Sensitivity in the Cancer database [31]. Then, the correlation analysis was conducted to assess the correlation between the risk score and the IC50 of drugs. When the absolute value of correlation coefficient between the risk score and IC50 of one drug is larger than 0.5 with a *P*-value <0.05, we considered that the risk score may have the ability to predict the sensitivity of this drug.

3. Results

3.1. Identification of prognostic IRGs

Firstly, we obtained 394 protein-coding IRGs with relevant scores$>$ 5 based on the GeneCards database. Following that, a univariate Cox analysis was conducted, which revealed 245 IRGs that were linked to the overall survival (OS) of patients with LGG in TCGA (Supplementary Table S2). Next, the functional enrichment analysis was conducted to investigate the underlying mechanisms of these 245 IRGs. The result of GO enrichment analysis showed that these 245 prognostic IRGs were significantly enriched in the

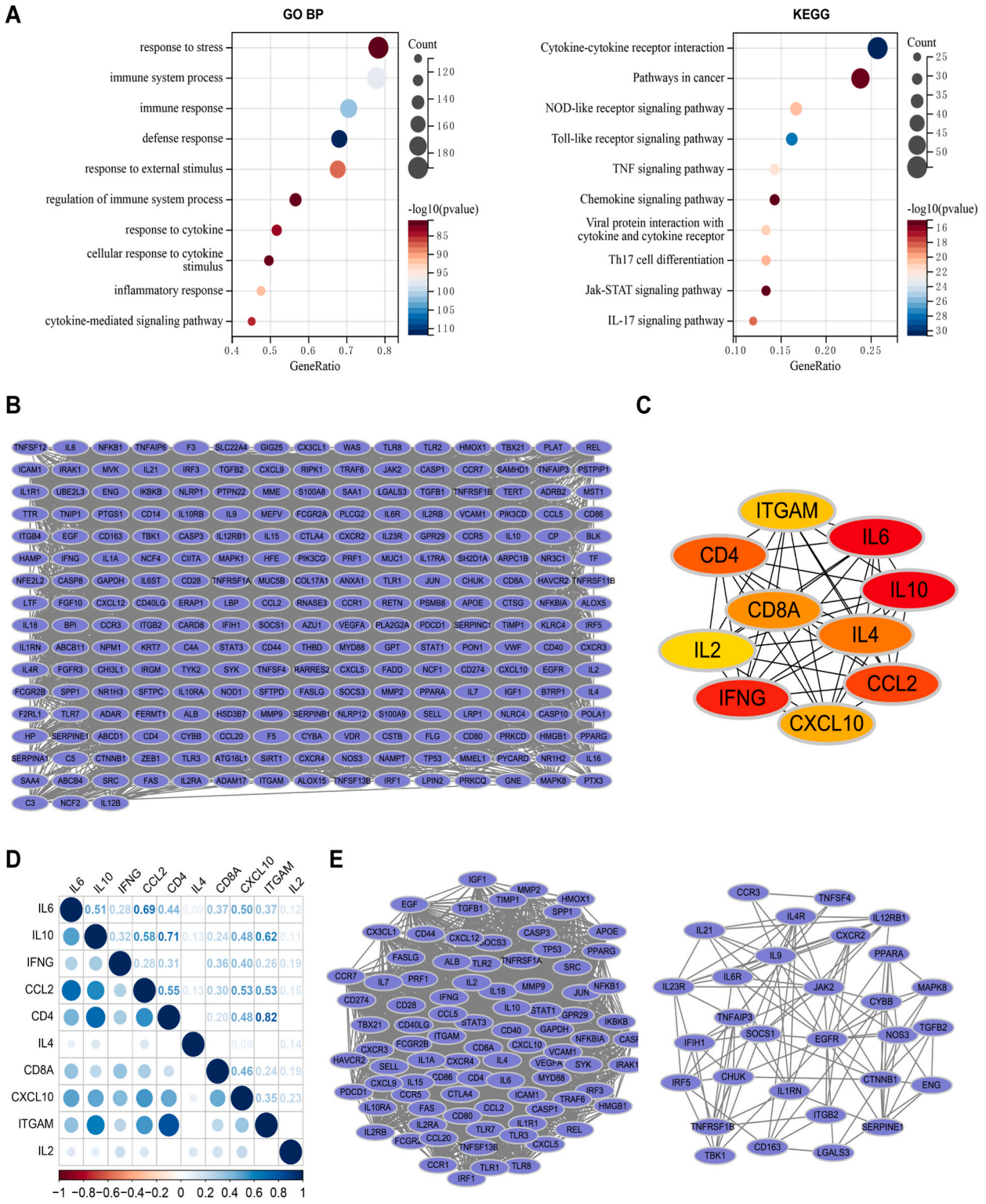

Fig. 1. Identification of prognostic IRGs and functional enrichment analysis. A. The top 10 enriched terms in GO analysis belonged to BP and KEGG analysis. **B.** PPI network of the DE-IRGs based on the STRING database. **C.** The hub genes obtained from the "cytohubba" plugin in Cytoscape software. **D.** The correlations between the hub IRGs. **E.** The two modules obtained from the "MCODE" plugin in Cytoscape software.

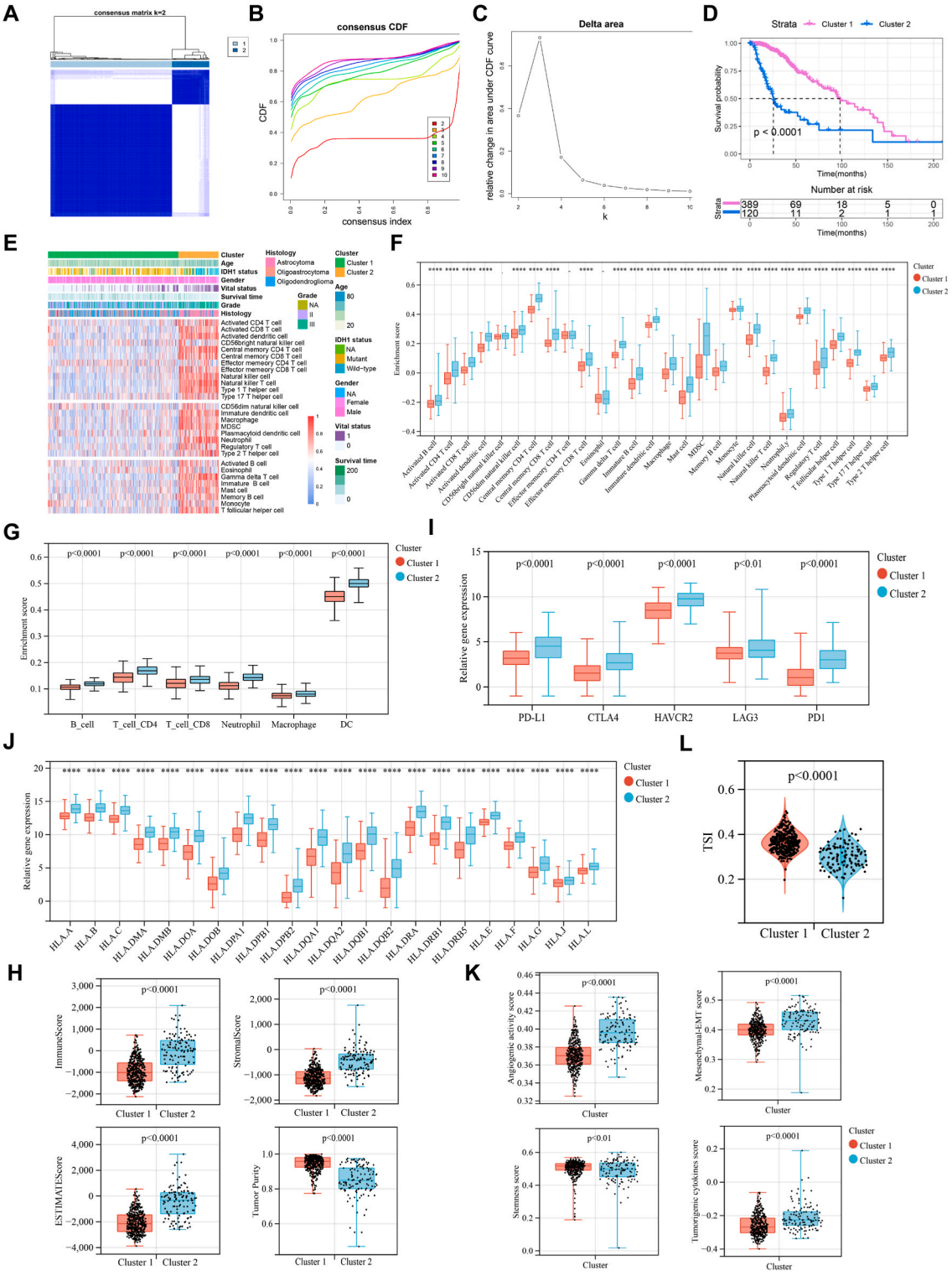

Fig. 2. Identification of Inflammation-Associated Clusters. A. Consensus clustering matrix (k = 2). **B.** Consensus clustering CDF diagram when k is valued from 2 to 10. **C.** Relative change in the area under the CDF curve for k ranged from 2 to 10. **D.** K-M curve depicts the OS difference between Cluster1 and Cluster2. **E.** Heatmap showed the relationship between clusters and 28 immune cells based on the TCGA-LGG cohort. Clinicopathological and molecular characteristics, including age, gender, vital status, OS time, histologic subtype, WHO grade, and IDH1 status, are shown as annotations. **F.** Boxplots showed the infiltration levels of 28 immune cells between Cluster1 and Cluster2 based on ssGSEA. **G.** Boxplots showed the infiltration levels of six immune cells between Cluster1 and Cluster2 based on TIMER. **H.** Boxplots showed the mRNA expression of five immune

checkpoint inhibitors between Cluster1 and Cluster2. **I.** Boxplots showed the mRNA expression of HLA genes between Cluster1 and Cluster2. **J.** Comparison of Immune Score, Stromal Score, ESTIMATE Score, and tumor purity between Cluster1 and Cluster2. **K.** Comparison of angiogenic activity, mesenchymal-EMT, tumourigenic cytokines, and stemness scores between Cluster1 and Cluster2. **L.** Comparison of TSI between Cluster1 and Cluster2.

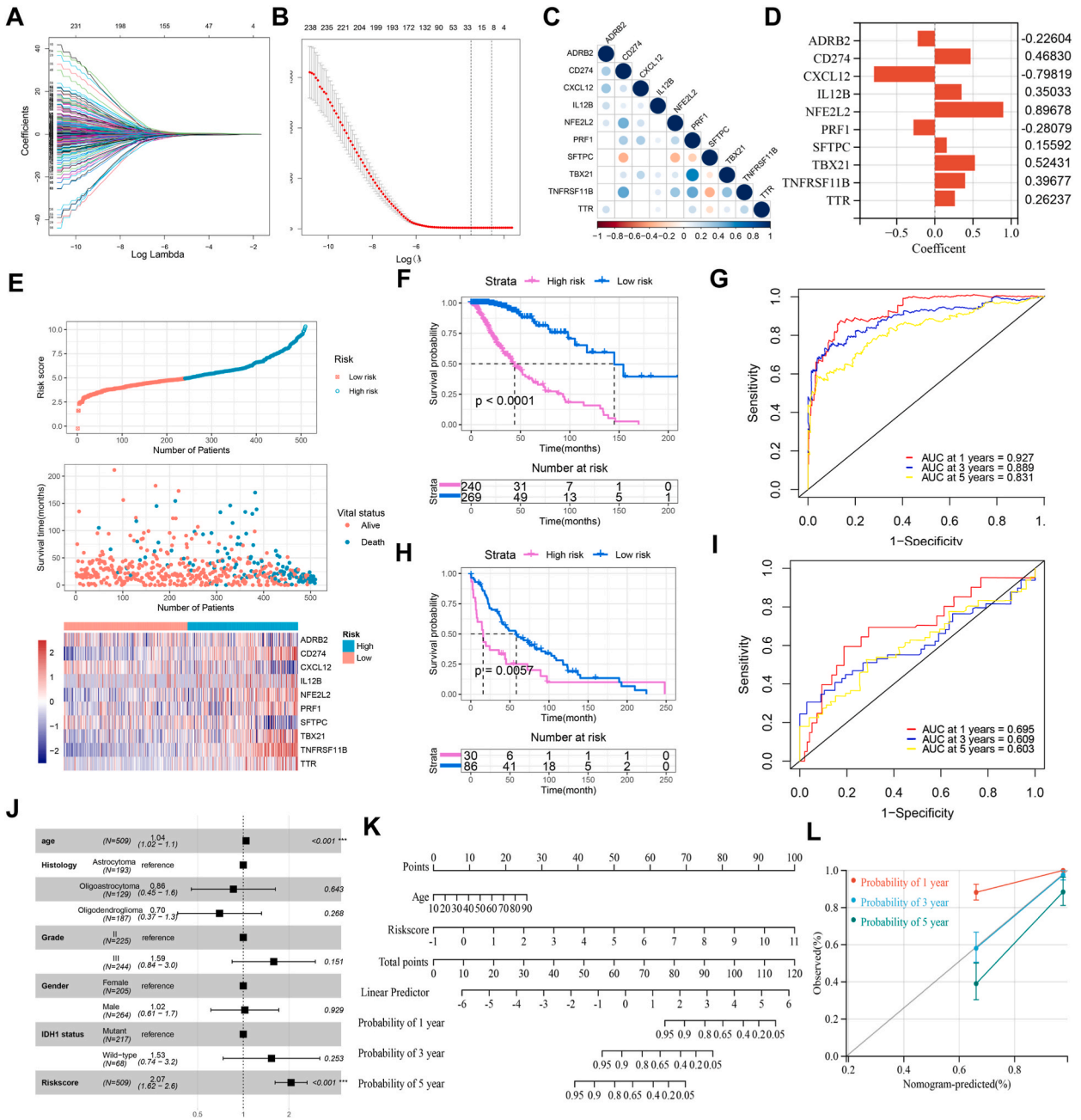

Fig. 3. Construction and validation of risk model. A. LASSO coefficient profiles of 245 prognostic IRGs. **B.** Ten-time cross-validation for tuning parameter selection in the LASSO model. **C.** Correlation analysis of 10 selected prognostic IRGs in the risk model. **D.** Coefficients for the 10 selected prognostic IRGs in the risk model. **E.** The distribution of risk score, survival status, and survival time and the heatmap of 10 model IRGs in the TCGA-LGG cohort. **F.** K-M curve for OS in TCGA-LGG cohort stratified by risk score. **G.** Time-dependent ROC curve for risk model in TCGA-LGG cohort. **H.** K-M curve for OS in GSE16011 cohort stratified by risk score **I.** Time-dependent ROC curves for risk model in GSE16011 cohort. **J.** The forest plot shows the multivariate Cox regression analysis using age, histological subtype, WHO grade, gender, IDH1 status, and risk score as covariates in the TCGA-LGG cohort. **K.** Nomogram based on age and risk score in TCGA-LGG cohort. **L.** Calibration plot of the nomogram for predicting the probability of 1-, 3- and 5-year survival.

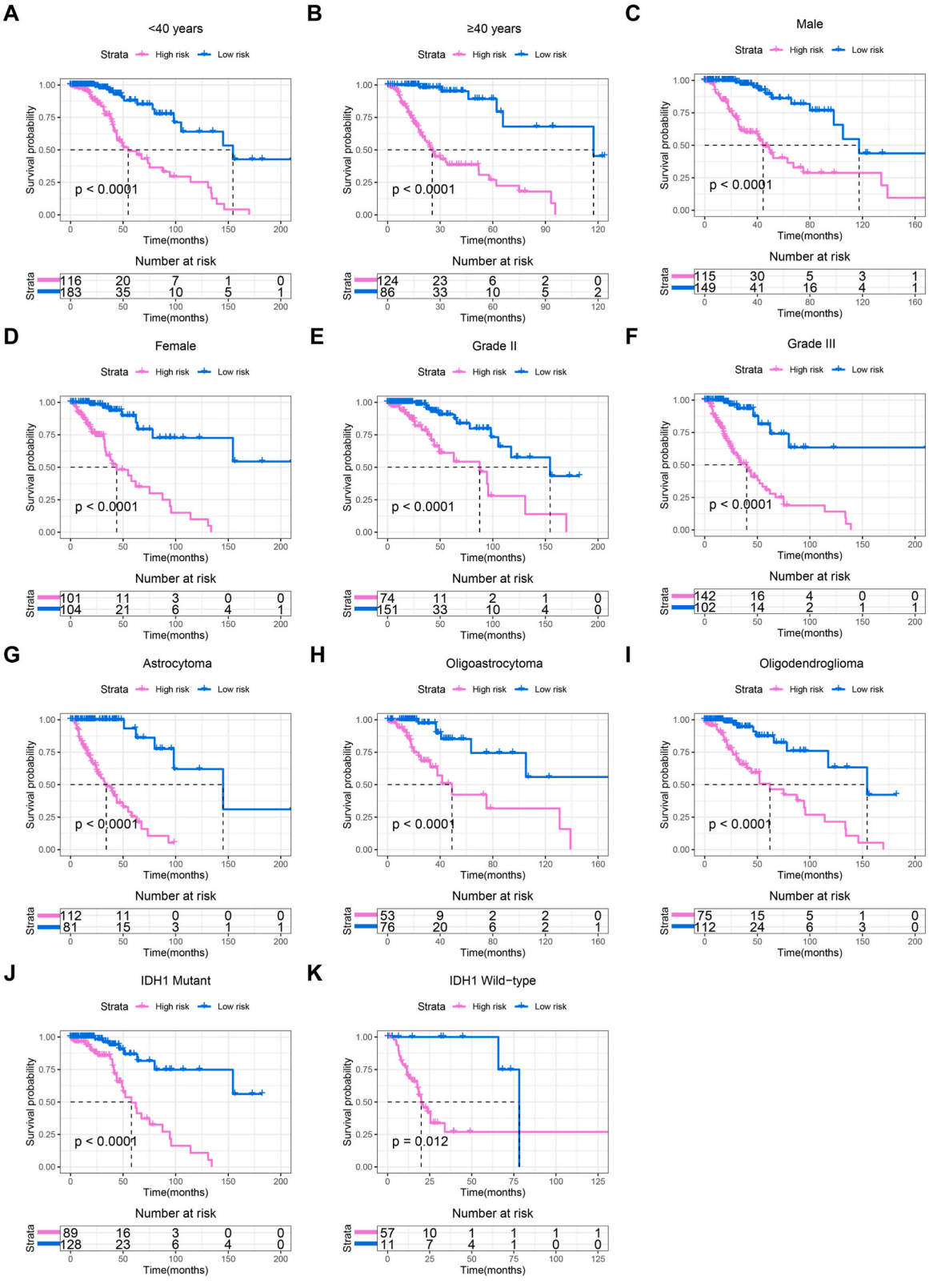

(caption on next page)

Fig. 4. Stratification analysis based on the risk model in the TCGA-LGG cohort. A, B. Stratified OS analysis in patients with different ages based on the risk model. **C, D.** Stratified OS analysis in patients with different genders based on the risk model. **E, F.** Stratified OS analysis in patients with different WHO grades based on the risk model. **G, I.** Stratified OS analysis in patients with different histological types based on the risk model. **J, K.** Stratified OS analysis in patients with different IDH1 status based on the risk model.

inflammatory response, immune response, response to cytokine, and other tumor-related processes (Fig. 1A). The result of KEGG pathway analysis showed that they were significantly enriched in cytokine-cytokine receptor interaction, NOD-like receptor and Toll-like receptor signaling pathways, chemokine signaling pathway, Th17 cell differential, TNF signaling and other tumor-related pathways (Fig. 1A). The analysis of the PPI network was conducted using the STRING database and visualized through the utilization of the

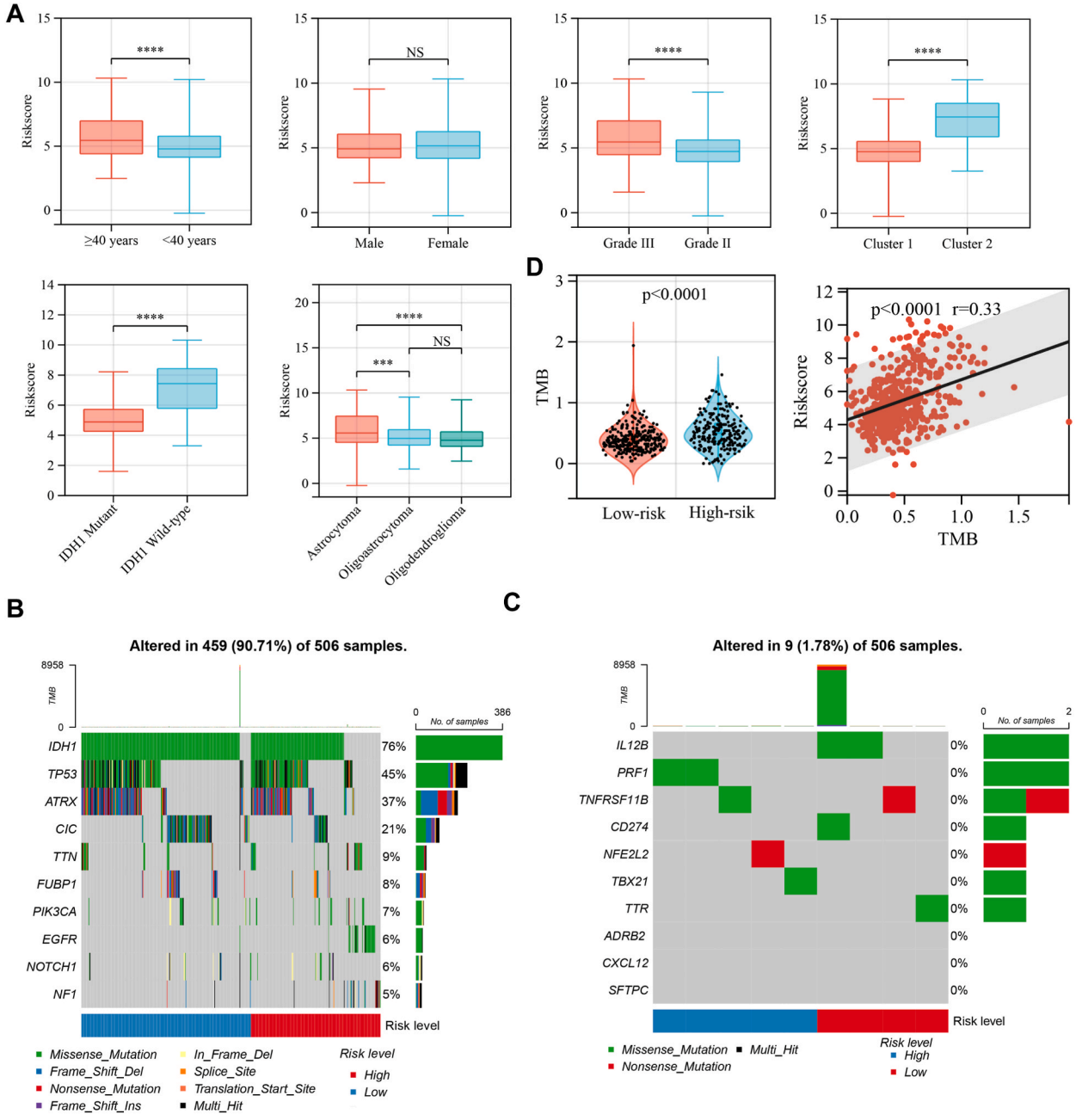

Fig. 5. The clinical and mutational characteristics of the risk model. A. Box plot showed differences in risk score between different clinical, histopathological, and molecular subtypes. **B.** Comparison of TMB between high- and low-risk groups and the correlation between TMB and risk score. **C.** The top 10 frequently mutated genes in high- and low-risk groups. **D.** The mutation of 10 IRGs between high- and low-risk groups.

Cytoscape software (Fig. 1B). Ranked with the degree, 10 hub genes were identified (Fig. 1C). The correlation analysis showed that the expression of hub genes was correlated positively (Fig. 1D). Additionally, we identified two modules formed by these genes based on MCODE (Fig. 1E).

3.2. Identification of two Inflammation-Associated Clusters in LGG

The 245 selected IRGs were used for cluster analysis. Patients with LGG were clustered into two groups (Fig. 2A–C). The Kaplan-Meier (K-M) curves showed that the OS of Cluster1 was better than Cluster2 (Fig. 2D). The clusters were significantly associated with clinicopathological and molecular parameters, including age, histology, grade, and IDH1 status (Fig. 2E). Moreover, we employed various algorithms to evaluate the levels of immune cell infiltration in these two clusters and performed a comparative analysis to examine the disparity in immune cell infiltration patterns between the two clusters. Based on the ssGSEA algorithm, the infiltration level of 28 immune cells in the two clusters was estimated. The differential analysis showed the infiltrative level of most immune cells in cluster2 was notably higher than that in cluster1 (Fig. 2E and F). Similarly, in the TIMER algorithm, cluster2 had higher infiltration levels of six immune cells than cluster1 (Fig. 2G). Based on the ESTIMATE algorithm, cluster2 had a remarkably higher ImmuneScore, StromalScore, and ESTIMATEScore, whereas, had lower tumor purity than cluster1 (Fig. 2H). Furthermore, we performed differential analysis and found that the expression of HLA and immune checkpoint genes in cluster2 was higher than that in cluster1 (Fig. 2I and J). In addition, we compared the tumorigenesis scores and TSIs between these two clusters and found that cluster2 exhibited notably elevated scores in angiogenic activity, mesenchymal EMT and tumorigenic cytokines. Conversely, cluster2 displayed lower scores in stemness and TSIs compared to cluster1 (Fig. 2K-L).

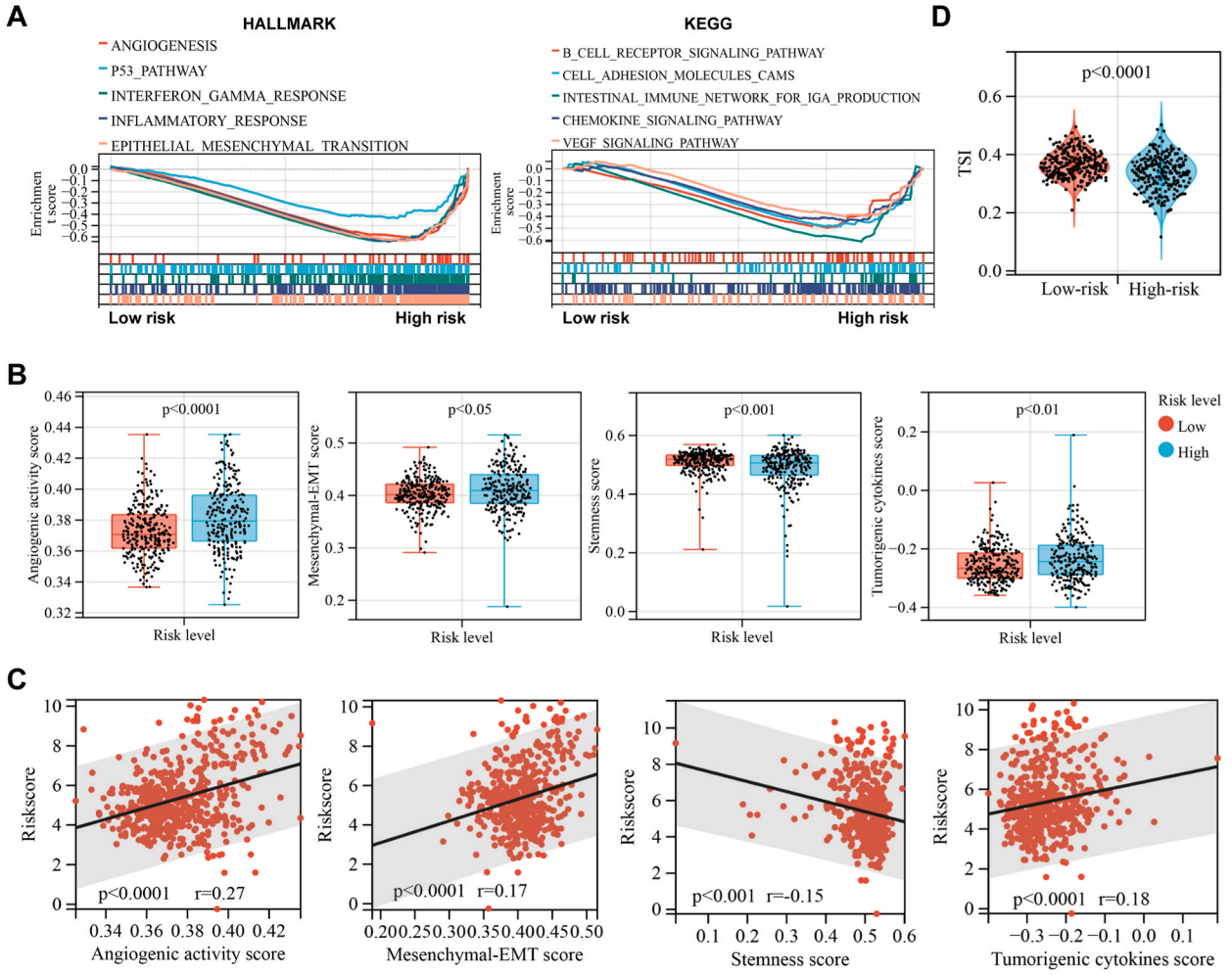

Fig. 6. The molecular characteristics of risk model. A. The enriched terms of HALLMARK and KEGG based on GSEA. **B.** Comparison of TSI between high- and low-risk groups. **C.** Comparison of angiogenic activity, mesenchymal-EMT, tumourigenic cytokines, and stemness scores between high- and low-risk groups **D.** The correlation between risk score and angiogenic activity, mesenchymal-EMT, tumourigenic cytokines, and stemness scores.

3.3. Construction and validation of the IRGs signature for LGG

To further identify some critical prognostic IRGs, the LASSO Cox analysis, and multivariable Cox regression were performed. Finally, 10 IRGs (ADRB2, CD274, CXCL12, IL12B, NFE2L2, PRF1, SFTPC, TBX21, TNFRSF11B, and TTR) were selected to construct an IRGs signature in TCGA-LGG cohort (Fig. 3A and B). The K-M curves showed that the 10 IRGs were associated with the OS of patients with LGG (Supplementary Fig. S2). There were general correlations between the expression of these 10 IRGs. (Fig. 3C). The coefficients

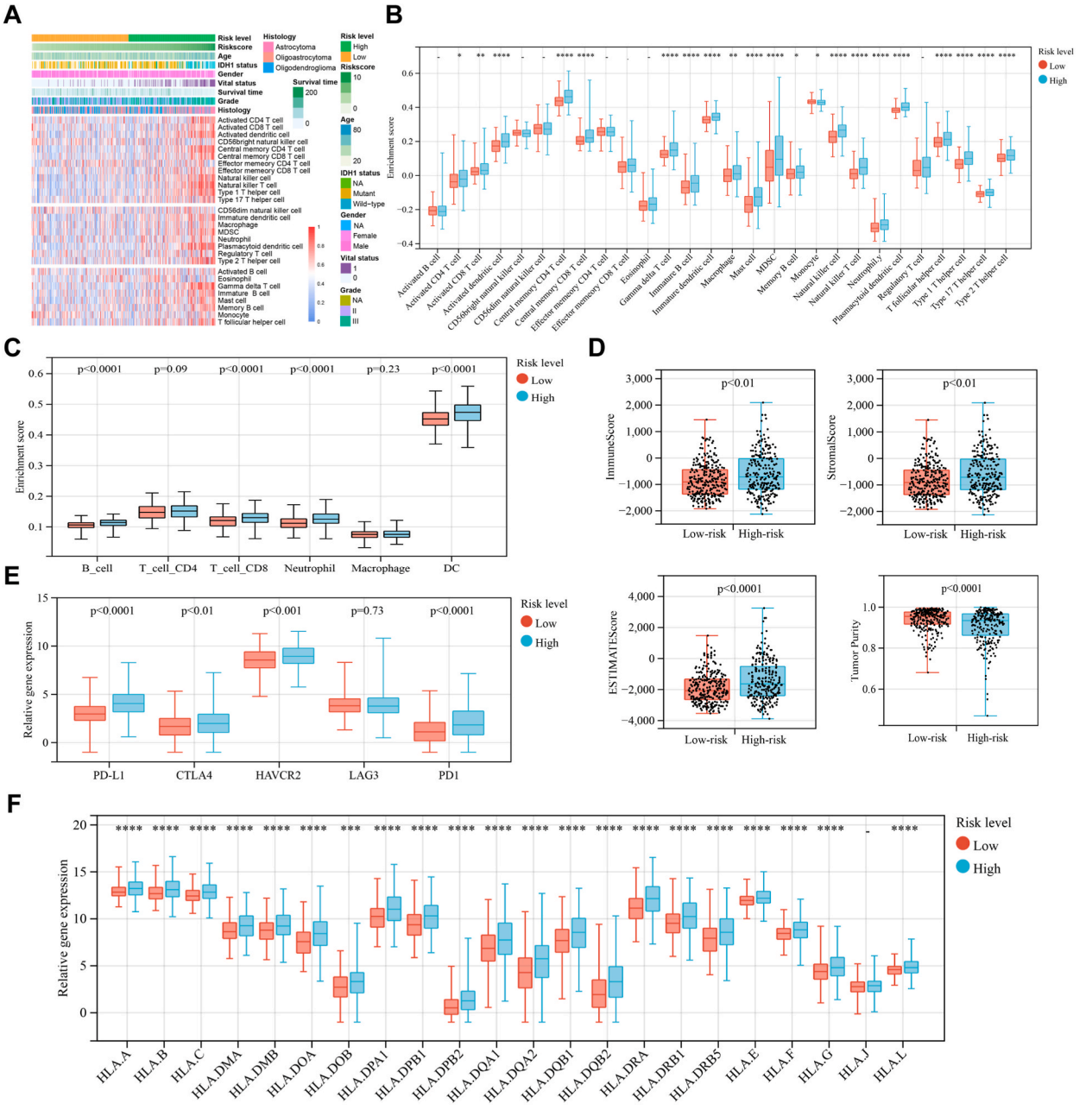

Fig. 7. The risk score associated with the immune cell infiltration and immune checkpoint inhibitors. A. Heatmap showed the relationship between risk score and 28 immune cells. Clinicopathological and molecular characteristics, including Age, gender, vital status, OS time, histologic subtype, WHO grade, and IDH1 status, are shown as annotations. **B.** Boxplot shows the differences of 28 immune cell infiltration between high- and low-risk groups based on ssGSEA. **C.** Boxplot shows the differences of six immune cell infiltration between high- and low-risk groups based on TIMER. **D.** Comparison of Immune Score, Stromal Score, ESTIMATE Score, and tumor purity between high- and low-risk groups. **E.** Boxplot shows the mRNA expression of five immune checkpoint inhibitors between high- and low-risk groups. **F.** Boxplot shows the mRNA expression of HLA genes between high- and low-risk groups.

of these 10 genes are presented in Fig. 3D. In the TCGA-LGG dataset, we divided the patients into high- and low-risk groups. Fig. 3E displays the distribution of risk score, OS time, survival status, and the expression pattern of the 10 IRGs among the two risk groups. The K-M curve revealed a significant disparity in the clinical outcome between the two risk groups, with patients in the high-risk group experiencing the shorter OS time compared to those in the low-risk group (Fig. 3F). Moreover, ROC curves indicated that the AUC for 1-year, 3-year, and 5-year OS time were 0.927, 0.889, and 0.831 correspondingly. This implies that the IRGs signature demonstrated an outstanding ability to forecast the patients' prognosis in the TCGA-LGG dataset (Fig. 3G). We obtained similar results in the GSE16011 dataset (Fig. 3H and I). In addition, we sequentially performed univariate and multivariate Cox analysis, which demonstrated that the IRGs signature was an independent risk factor in LGG (Supplementary Table S3 and Fig. 3J). Furthermore, we constructed a nomogram

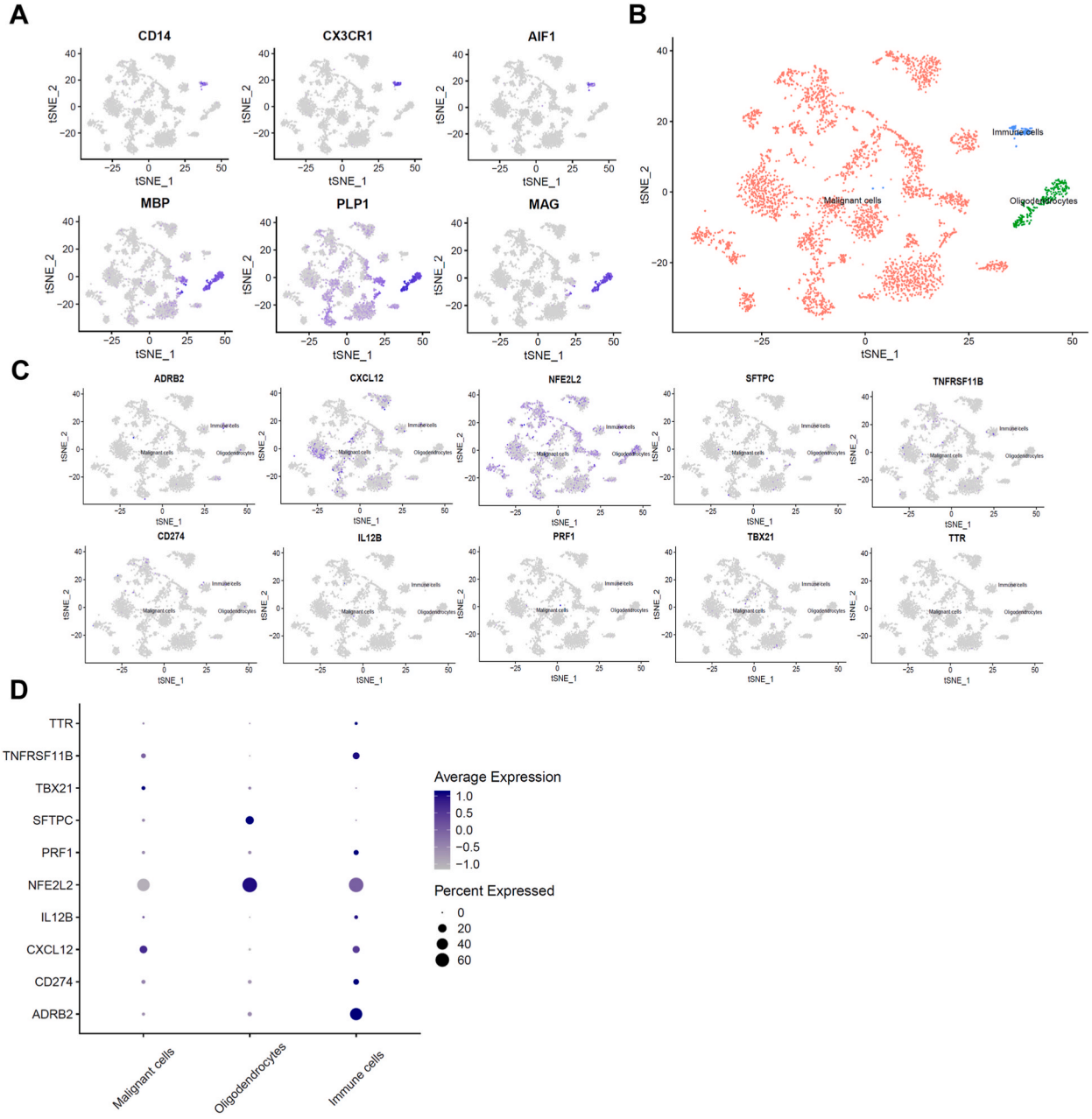

Fig. 8. The scRNA-seq analysis of 10 IRGs. A. Feature plots for cell markers in glioma. The color indicates the average expression level of markers. **B.** The t-SNE plot of the three main cell types in glioma. **C.** Feature plots for 10 IRGs in glioma. The color indicates the average expression level of IRGs. **D.** The dot plot shows the expression of 10 IRGs in three cell types. The size of the dots indicates the proportion of cells expressing a specific IRG, and the color indicates the average expression level of the IRG. (For interpretation of the references to color in this figure legend, the reader is referred to the Web version of this article.)

model, including age and IRGs signature (Fig. 3K). The calibration plot of the nomogram was also drawn and the results demonstrated that the predicted times of the nomogram were highly consistent with actual 1-year, 3-year, and 5-year OS time (Fig. 3L).

Subsequently, we performed a stratification analysis of the IRGs signature in both clinical and molecular subgroups. The analysis revealed that individuals with LGG in the high-risk group consistently experienced a shorter OS time (Fig. 4A–K).

3.4. Clinical and mutational characteristics of the IRGs signature

First, the distribution pattern of IRGs signature in these subgroups were plotted and the difference between subgroups was compared (Fig. 5A). The risk score for patients with age ≥40 years, grade III, cluster2, IDH1-WT, and astrocytoma was significantly higher than that for patients belonging to other subtypes, which suggested that IRGs signature was significantly correlated with age, WHO grade, inflammation-molecular subtypes, histological types, and IDH1 status (Fig. 5A). Based on TCGA-LGG cohort, gene mutation analysis was performed and the top 10 mutant genes, such as IDH1, TP53, and ATRX were presented (Fig. 5B). Furthermore, the mutation of 10 IRGs in TCGA-LGG cohort was also analyzed and the 10 IRGs were barely mutated in LGG (Fig. 5C). Furthermore, we compared the TMB of patients with LGG between two risk groups and found that TMB for high-risk patients was notably higher than that for low-risk patients (Fig. 5D). Consistently, the correlation between risk score and TMB was positive with statistically significant (Fig. 5D).

3.5. Molecular characteristics of the current risk model

GSEA was conducted to explore the underlying mechanism of the risk score. The results showed that high-risk patients with LGG had enriched in pro-cancer-related pathways, such as the EMT, angiogenesis, VEGF, and P53 pathways, as well as immune-related pathways, including the cell adhesion, chemokine signaling pathway, and inflammatory response (Fig. 6A). Subsequently, we compared the difference of tumorigenesis scores between the two risk groups and found that patients with high risk score had significantly higher enrichment scores in angiogenic activity, mesenchymal EMT, and tumorigenic cytokines, however, lower enrichment score in stemness than patients with low risk score (Fig. 6B). Furthermore, Pearson's correlation coefficients between risk score and tumorigenesis scores were respectively calculated and the results showed that three scores, including angiogenesis ($R = 0.27$, $p < 0.0001$), mesenchymal EMT ($R = 0.17$, $p < 0.0001$), and tumorigenic cytokine scores ($R = 0.18$, $p < 0.0001$), were positively correlated with the IRGs signature score, whereas, stemness score ($R = -0.15$, $p < 0.0001$) was negatively correlated with the IRGs signature score (Fig. 6C). Furthermore, we compared the TSIs between the two risk groups and found that the high-risk patients had lower TSIs than low-risk patients (Fig. 6D).

3.6. IRGs signature correlated with the immune cell infiltration in LGG

Our previous analyses have suggested that our risk score significantly enriched immune-related pathways. Therefore, we further investigated and compared the infiltration pattern of immune cells between patients within these two risk groups. The immune infiltration of LGG patients in the risk groups was respectively estimated by using several algorithms, including ssGSEA, TIMER, and

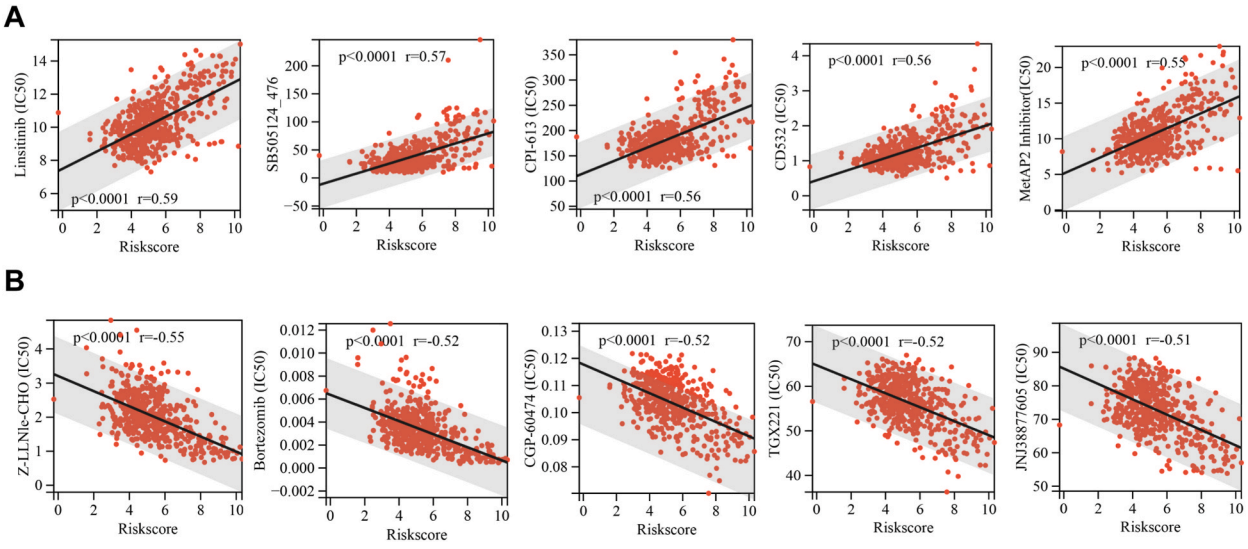

Fig. 9. The risk score predicted the chemotherapy response. A. The risk score positively correlated with the IC50 of Linstinib, SB505124_476, CPI-613, CD532, and MetAP2 inhibitor. **B.** The risk score negatively correlated with the IC50 of Z-LLNle-CHO, Bortezomib, CGP-60474, TGX221, and JNJ38877605.

ESTIMATE algorithms. Based on the ssGSEA algorithm, 28 immune cells infiltrated in the TME of LGG in the two risk groups were assessed. The result indicated that these two risk groups had notably different infiltration pattern of these 28 cells (Fig. 7A). For most of these 28 cells, the infiltration levels in high-risk group were remarkably higher than the levels in low-risk group (Fig. 7B). Similarly, the infiltration levels of dendritic cells, neutrophils, B cells, and $CD8^+$ T cells in high-risk patients were significantly higher, however, the difference of infiltration levels of $CD4^+$ T cell and macrophage was not statistically significant based on the TIMER algorithm (Fig. 7C). Based on the ESTAMATE algorithm, the patients with high risk score had remarkably higher ImmuneScore, StromalScore, and ESITIMATEScore, whereas, had lower tumor purity than patients with low risk score (Fig. 7D). Further, we performed differential analysis and found that expression of HLA and immune checkpoint genes in high-risk group was higher (Fig. 7E and F).

In further scRNA-seq analyses, we annotated single cells from six glioma samples as malignant cells, oligodendrocytes, and immune cells based on cell markers from the previous publication (Fig. 8A and B) [19]. We analyzed the expression of 10 IRGs in different cells and found that ADRB2, CD274, IL12B, PRF1, TNFRSF11B, and TTR were highly expressed in immune cells; TBX21 was highly expressed in malignant cells; SFTPC was highly expressed in oligodendrocytes; CXCL12 was highly expressed in both malignant and immune cells and NFE2L2 was highly expressed in both oligodendrocytes and immune cells (Fig. 8C and D).

3.7. Risk score predicted the chemotherapy response

To explore the ability of the IRGs signature to predict the response of chemotherapy drugs, the "pRRophetic" method was used to predict the IC50 values of chemotherapeutic agents in patients with LGG and found that there was a correlation between the IRGs signature score and the sensitivity of 10 drugs. It was shown that the IRGs signature had a significantly positive correlation with IC50 of Linstinib, SB505124_476, CPI-613, CD532, and MetAP2 inhibitor (Fig. 9A, $R > 0.5$, $p < 0.05$), whereas, negative correlation with Z-LLNle-CHO, Bortezomib, CGP-60474, TGX221, and JNJ38877605 (Fig. 9B, $R < -0.5$, $p < 0.05$). The targets of these 10 drugs are shown in Supplementary Table S4.

4. Discussion

An inflammatory microenvironment is an essential component of TME. Many studies have demonstrated that inflammation involves the initiation and progression of various cancers, including LGG [32]. Several studies have demonstrated that inflammatory genes are frequently dysregulated in both serum and tumor specimens, play multifaceted roles in various tumors, and are potentially novel biomarkers [33]. Therefore, it is feasible to identify biomarkers based on IRGs for LGG. This study conducted thorough examinations to assess the prognosis significance of IRGs, identify potential biomarkers, and construct a predictive risk model in LGG.

It was found that most of IRGs were associated with the prognosis of LGG patients. These 245 prognostic IRGs were significantly enriched in the inflammatory response, immune response-related pathways, Th17 cell differential, TNF signaling, and other tumor-related processes and pathways. Furthermore, patients with LGG could be clustered into subgroups based on these prognostic IRGs, and the patients in the two clusters presented different survival time, immune cell infiltration, tumorigenesis scores, and TSIs. These results indicated that inflammation was related to the prognosis and tumorigenesis of LGG. Indeed, the relationship between inflammation and glioma has been revealed by an increasing number of studies. For instance, epidemiological studies indicated that inflammation is associated with the occurrence of glioma [34]. Song et al. [35] have reported that inflammation is associated with behavioral symptoms in patients with glioma. Emerging studies have suggested that inflammatory markers, such as NLR and PLR, are correlated with the prognosis of glioma [36,37]. In the past few years, a growing body of evidence has proved that inflammatory cells (microglia, macrophages, etc.), inflammatory factors (IL6, IL8, TNF-α, etc.), and inflammation-related pathways (NF–κB, STAT3, etc.) are involved in the progression of glioma and correlated with prognosis [38–40]. Therefore, our work enhances comprehension of inflammation in LGG and provides clues for identifying new biomarkers for LGG.

Furthermore, we screened 10 potential and critical prognostic IRGs for LGG, including ADRB2, CD274, CXCL12, IL12B, NFE2L2, PRF1, SFTPC, TBX21, TNFRSF11B, and TTR. Certain IRGs have been documented to have crucial functions in glioma. CD274, also known as PD-L1, is widely used as a candidate biomarker for predicting the response to anti-immune checkpoint immunotherapy [41]. In recent years, many studies have reported that the expression of PD-L1 is aberrantly increased in glioma, positively correlated with grades, and associated with glioma genotypes [42,43]. Although anti-immune checkpoint immunotherapy for gliomas has not been implemented in clinical practice, existing clinical trials have confirmed the potential survival benefits of PD-1 immunotherapy for some glioma patients [44]. Therefore, our identified CD274 can serve not only as a prognostic biomarker but also as a possible guide for future immunotherapy in glioma. CXCL12 is a homeostatic chemokine that binds primarily to the CXC receptor 4 (CXCR4). Many studies have illustrated that the CXCL12/CXCR4 axis regulates various signaling pathways including the ERK pathway, to participate in tumorigenesis [45]. Previous studies have also reported that this axis is upregulated in the TME of glioma, regulates glioma cell proliferation, invasion, and angiogenesis, and influences the efficacy of radio-chemotherapy [46]. For example, Anália do Carmo et al. have reported that the CXCL12/CXCR4 axis promotes glioma cell proliferation and motility [47]. Furthermore, the CXCL12/CXCR4 axis regulates TMZ resistance in glioma, and inhibition of CXCL12/CXCR4 signaling increases the TMZ sensitivity in glioma cells [48]. Therefore, besides serving as a prognostic biomarker, further exploration of the potential of CXCL12 as a marker for chemotherapy response is promising. Regarding IL12B, a study has suggested that the interaction between IL12B and IL12A may be related to the susceptibility of brain tumors [49]. Erythroid 2-like 2 (NFE2L2), a nuclear factor, is a transcription factor and regulates oxidative stress and inflammatory response. Several studies have reported that NFE2L2 is involved in the tumorigenesis of various cancers, such as hepatocellular carcinoma, breast cancer, esophageal cancer, and endometrial cancer [50]. Recently, Luo et al. have demonstrated that LINC01564 increases TMZ resistance in glioma cells and inhibits ferroptosis by upregulating NFE2L2 expression, which provides a

novel perspective on TMZ resistance in glioma [51]. Through a pan-cancer analysis, Ju et al. have reported that NFE2L2 is correlated with immune infiltration and is a potential biomarker in LGG [52]. These studies provide a theoretical basis for NFE2L2 as a prognostic biomarker and a marker of chemotherapy sensitivity. TNFRSF11B, full name is Tumor necrosis factor (TNF) receptor superfamily member 11B, is a member of the TNF receptor superfamily and is involved in the tumorigenesis of several human cancers, such as gastric and breast cancers [53,54]. A previous study showed that the inhibition of the activity of IRE1 deregulates TNF receptor superfamily genes, including TNFRSF11B, to slow glioma cell growth [55]. Notably, our scRNA-seq analysis also confirmed that most of these 10 IRGs were highly expressed in immune cells, suggesting the possibility that these IRGs act as immune regulators. Overall, many studies have confirmed the potential of the IRGs we identified as prognostic biomarkers, markers of chemotherapy response, and immunotherapy markers. Further study of these 10 prognostic IRGs is valuable and beneficial for guiding personalized and targeted therapeutic interventions, especially those genes that have not been extensively investigated in gliomas.

The outcome and how patients with LGG respond to treatment differ significantly, which cannot be precisely predicted by clinicopathological characteristics and known genetic biomarkers [56,57]. Risk stratification plays an important role and is essential for the management of patients with cancers and the development of individualized treatment [58]. In this study, multivariate Cox and stratified analyses revealed that our IRGs signature is not only an independent risk factor but can also identify patients with poor outcomes in different histological and molecular subgroups. The prognosis of LGG patients with high IRGs signature scores was always shorter than that of patients with low IRGs signature scores. Therefore, the risk model is useful for predicting the survival in LGG and identifying those who need aggressive treatment. In recent decades, immunotherapy has become a powerful clinical strategy for cancer treatment. However, owing to its serious adverse effects, broad implementation of immunotherapy for cancer remains difficult [59]. Improving the response rate to immunotherapy is a key problem in immunotherapy. Increasing clinical research has confirmed that immune cell infiltration in the TME has predictive value in prognosis and immunotherapy in cancers [60]. Previous studies have indicated that the immunotherapy response also correlates with TMB and the expression of immune checkpoint genes [61,62]. Here, we demonstrated that our risk score was related to the infiltration level of immune cells, especially the immunosuppressive cells. Furthermore, the IRGs signature was closely correlated with TMB and the expression of immune checkpoint inhibitors. All of these results suggest that IRGs signature may have the ability to predict the response of immunotherapy in LGG. Moreover, we also found a significant correlation between risk score and IC50 value of several drugs, including linstinib, SB505124_476, CPI-613, CD532, MetAP2 inhibitor, Z-LLNle-CHO, bortezomib, CGP-60474, TGX221, and JNJ38877605. Therefore, our risk model may have the potential to guide individual treatment in patients with LGG.

However, this study still has several limitations. First, the datasets used to validate our signature are retrospective data. Second, the results need to be further confirmed by *in vivo* and *in vitro* experiments. Third, immune cell infiltration and IC50 were estimated using algorithms. In the future, sufficient samples of LGG should be collected to verify the value of this model and more validations should be performed to investigate the function of the selected IRGs in LGG.

5. Conclusion

In this study, we screened 245 prognostic IRGs, identified two inflammation-associated molecular clusters, and established a prognostic risk model based on 10 prognostic IRGs. The risk model significantly correlated with the infiltration level of immune cells, TMB, TSIs, tumorigenesis scores, and expression of immune checkpoint inhibitors and HLA genes in LGG. Additionally, the risk model could predict the response of several drugs in LGG. This study promoted the development of individualized treatment to enhance the clinical outcomes of LGG.

Funding

This study was supported by one grant from the China Postdoctoral Science Foundation (No. 2023M733960) and one grant from National Natural Science Foundation of China (No. 82303253).

Data availability

Data included in article/supp. material/referenced in article.

Consent for publication

Not applicable.

Ethics statement

Not applicable.

CRediT authorship contribution statement

Cheng Long: Data curation, Investigation, Methodology, Visualization, Writing – original draft. **Ya Song:** Methodology, Writing – review & editing. **Yimin Pan:** Conceptualization, Methodology, Visualization, Writing – review & editing. **Changwu Wu:**

Conceptualization, Data curation, Funding acquisition, Investigation, Methodology, Software, Supervision, Writing – review & editing.

Declaration of competing interest

The authors declare that they have no known competing financial interests or personal relationships that could have appeared to influence the work reported in this paper.

Acknowledgements

The results shown here are in part based upon data generated by TCGA (http://cancergenome.nih.gov) and the GEO database (https://www.ncbi.nlm.nih.gov/geo/). We also appreciate the convenience of visualization provided by the web tool Sangerbox (http://sangerbox.com/Tool).

Abbreviations

LGG	Lower grade gliomas
IRG	Inflammation-related gene
TCGA	The Cancer Genome Atlas
WHO	World Health Organization
GBM	Glioblastoma
TME	Tumor microenvironment
GEO	Gene Expression Omnibus
GSEA	Gene Set Enrichment Analysis
ssGSEA	Single Sample Gene Set Enrichment Analysis
GO	Gene Oncology
KEGG	Kyoto Encyclopedia of Genes and Genomes
TMB	Tumor Mutation Burden
TSI	Tumor Stemness Indice
OS	Overall survival
scRNA-seq	Single-cell RNA sequencing

Appendix A. Supplementary data

Supplementary data to this article can be found online at https://doi.org/10.1016/j.heliyon.2023.e22429.

References

[1] S.H. Patel, et al., T2-FLAIR mismatch, an imaging biomarker for IDH and 1p/19q status in lower-grade gliomas: a TCGA/TCIA project, Clin. Cancer Res. : an official journal of the American Association for Cancer Research 23 (2017) 6078–6085, https://doi.org/10.1158/1078-0432.CCR-17-0560.
[2] N. Cancer Genome Atlas Research, et al., Comprehensive, integrative genomic analysis of diffuse lower-grade gliomas, N. Engl. J. Med. 372 (2015) 2481–2498, https://doi.org/10.1056/NEJMoa1402121.
[3] P. Kumthekar, J. Raizer, S. Singh, Low-grade glioma, Cancer Treat Res. 163 (2015) 75–87, https://doi.org/10.1007/978-3-319-12048-5_5.
[4] H. Peng, et al., A risk model developed based on homologous recombination deficiency predicts overall survival in patients with lower grade glioma, Front. Genet. 13 (2022), 919391, https://doi.org/10.3389/fgene.2022.919391.
[5] H. Duffau, Paradoxes of evidence-based medicine in lower-grade glioma: to treat the tumor or the patient? Neurology 91 (2018) 657–662, https://doi.org/10.1212/WNL.0000000000006288.
[6] S. Chen, Y. Sun, X. Zhu, Z. Mo, Prediction of survival outcome in lower-grade glioma using a prognostic signature with 33 immune-related gene pairs, Int. J. Gen. Med. 14 (2021) 8149–8160, https://doi.org/10.2147/IJGM.S338135.
[7] C. Wu, et al., A tumor microenvironment-based prognostic index for osteosarcoma, J. Biomed. Sci. 30 (2023) 23, https://doi.org/10.1186/s12929-023-00917-3.
[8] C. Wu, et al., Tumor antigens and immune subtypes of glioblastoma: the fundamentals of mRNA vaccine and individualized immunotherapy development, J Big Data 9 (2022) 92, https://doi.org/10.1186/s40537-022-00643-x.
[9] F.R. Greten, S.I. Grivennikov, Inflammation and cancer: triggers, mechanisms, and consequences, Immunity 51 (2019) 27–41, https://doi.org/10.1016/j.immuni.2019.06.025.
[10] A. Mantovani, P. Allavena, A. Sica, F. Balkwill, Cancer-related inflammation, Nature 454 (2008) 436–444, https://doi.org/10.1038/nature07205.
[11] M. Murata, Inflammation and cancer, Environ. Health Prev. Med. 23 (2018) 50, https://doi.org/10.1186/s12199-018-0740-1.
[12] N. Singh, et al., Inflammation and cancer, Ann. Afr. Med. 18 (2019) 121–126, https://doi.org/10.4103/aam.aam_56_18.
[13] P. Chiarugi, P. Cirri, Metabolic exchanges within tumor microenvironment, Cancer Lett. 380 (2016) 272–280, https://doi.org/10.1016/j.canlet.2015.10.027.
[14] N.A. Bhowmick, E.G. Neilson, H.L. Moses, Stromal fibroblasts in cancer initiation and progression, Nature 432 (2004) 332–337, https://doi.org/10.1038/nature03096.
[15] A. Orimo, et al., Stromal fibroblasts present in invasive human breast carcinomas promote tumor growth and angiogenesis through elevated SDF-1/CXCL12 secretion, Cell 121 (2005) 335–348, https://doi.org/10.1016/j.cell.2005.02.034.
[16] R.D. Schreiber, L.J. Old, M.J. Smyth, Cancer immunoediting: integrating immunity's roles in cancer suppression and promotion, Science 331 (2011) 1565–1570, https://doi.org/10.1126/science.1203486.
[17] Y. Ohue, H. Nishikawa, Regulatory T (Treg) cells in cancer: can Treg cells be a new therapeutic target? Cancer Sci. 110 (2019) 2080–2089, https://doi.org/10.1111/cas.14069.

[18] M.G. Morvan, L.L. Lanier, NK cells and cancer: you can teach innate cells new tricks, Nat. Rev. Cancer 16 (2016) 7–19, https://doi.org/10.1038/nrc.2015.5.
[19] M.G. Filbin, et al., Developmental and oncogenic programs in H3K27M gliomas dissected by single-cell RNA-seq, Science 360 (2018) 331–335, https://doi.org/10.1126/science.aao4750.
[20] R. Satija, J.A. Farrell, D. Gennert, A.F. Schier, A. Regev, Spatial reconstruction of single-cell gene expression data, Nat. Biotechnol. 33 (2015) 495–502, https://doi.org/10.1038/nbt.3192.
[21] A. Butler, P. Hoffman, P. Smibert, E. Papalexi, R. Satija, Integrating single-cell transcriptomic data across different conditions, technologies, and species, Nat. Biotechnol. 36 (2018) 411–420, https://doi.org/10.1038/nbt.4096.
[22] T. Stuart, et al., Comprehensive integration of single-cell data, Cell 177 (2019) 1888–1902, https://doi.org/10.1016/j.cell.2019.05.031, e1821.
[23] Y. Hao, et al., Integrated analysis of multimodal single-cell data, Cell 184 (2021) 3573–3587, https://doi.org/10.1016/j.cell.2021.04.048, e3529.
[24] H. Wickham, ggplot2: Elegant Graphics for Data Analysis, Springer-Verlag New York, 2016.
[25] C. Wu, et al., Liquid biopsy-based identification of prognostic and immunotherapeutically relevant gene signatures in lower grade glioma, Journal of Big Data 10 (2023) 19, https://doi.org/10.1186/s40537-023-00686-8.
[26] R. Tibshirani, The lasso method for variable selection in the Cox model, Stat. Med. 16 (1997) 385–395, https://doi.org/10.1002/(sici)1097-0258(19970228)16:4<385::aid-sim380>3.0.co;2-3.
[27] C. Qiu, et al., Identification of molecular subtypes and a prognostic signature based on inflammation-related genes in colon adenocarcinoma, Front. Immunol. 12 (2021), 769685, https://doi.org/10.3389/fimmu.2021.769685.
[28] K. Chen, et al., Immunological and prognostic analysis of PSENEN in low-grade gliomas: an immune infiltration-related prognostic biomarker, Front. Mol. Neurosci. 15 (2022), 933855, https://doi.org/10.3389/fnmol.2022.933855.
[29] T.M. Malta, et al., Machine learning identifies stemness features associated with oncogenic dedifferentiation, Cell 173 (2018) 338–354 e315, https://doi.org/10.1016/j.cell.2018.03.034.
[30] P. Geeleher, N. Cox, R.S. Huang, pRRophetic: an R package for prediction of clinical chemotherapeutic response from tumor gene expression levels, PLoS One 9 (2014), e107468, https://doi.org/10.1371/journal.pone.0107468.
[31] C. Wu, et al., Pan-cancer analyses reveal molecular and clinical characteristics of cuproptosis regulators, iMeta 2 (2023) e68, https://doi.org/10.1002/imt2.68.
[32] A. Cho, K.J. McKelvey, A. Lee, A.L. Hudson, The intertwined fates of inflammation and coagulation in glioma, Mamm. Genome : official journal of the International Mammalian Genome Society 29 (2018) 806–816, https://doi.org/10.1007/s00335-018-9761-8.
[33] Z.J. Liu, P.X. Hou, X.X. Wang, An inflammation-related nine-gene signature to improve prognosis prediction of lung adenocarcinoma, Disease markers 2021 (2021), 9568057, https://doi.org/10.1155/2021/9568057.
[34] R.P. Galvao, H. Zong, Inflammation and gliomagenesis: Bi-directional communication at early and late stages of tumor progression, Current pathobiology reports 1 (2013) 19–28, https://doi.org/10.1007/s40139-012-0006-3.
[35] L. Song, et al., Inflammation and behavioral symptoms in preoperational glioma patients: is depression, anxiety, and cognitive impairment related to markers of systemic inflammation? Brain and behavior 10 (2020), e01771 https://doi.org/10.1002/brb3.1771.
[36] M.G. McNamara, et al., Factors impacting survival following second surgery in patients with glioblastoma in the temozolomide treatment era, incorporating neutrophil/lymphocyte ratio and time to first progression, Journal of neuro-oncology 117 (2014) 147–152, https://doi.org/10.1007/s11060-014-1366-9.
[37] S. Han, et al., Pre-treatment neutrophil-to-lymphocyte ratio is associated with neutrophil and T-cell infiltration and predicts clinical outcome in patients with glioblastoma, BMC Cancer 15 (2015) 617, https://doi.org/10.1186/s12885-015-1629-7.
[38] S. Muller, et al., Single-cell profiling of human gliomas reveals macrophage ontogeny as a basis for regional differences in macrophage activation in the tumor microenvironment, Genome biology 18 (2017) 234, https://doi.org/10.1186/s13059-017-1362-4.
[39] J. Albrengues, et al., Neutrophil extracellular traps produced during inflammation awaken dormant cancer cells in mice, Science 361 (2018), https://doi.org/10.1126/science.aao4227.
[40] Q. Lei, et al., TNIP1-mediated TNF-alpha/NF-kappaB signalling cascade sustains glioma cell proliferation, J. Cell Mol. Med. 24 (2020) 530–538, https://doi.org/10.1111/jcmm.14760.
[41] A. Akinleye, Z. Rasool, Immune checkpoint inhibitors of PD-L1 as cancer therapeutics, J. Hematol. Oncol. 12 (2019) 92, https://doi.org/10.1186/s13045-019-0779-5.
[42] Z. Wang, et al., Molecular and clinical characterization of PD-L1 expression at transcriptional level via 976 samples of brain glioma, OncoImmunology 5 (2016), e1196310, https://doi.org/10.1080/2162402X.2016.1196310.
[43] S.T. Garber, et al., Immune checkpoint blockade as a potential therapeutic target: surveying CNS malignancies, Neuro Oncol. 18 (2016) 1357–1366, https://doi.org/10.1093/neuonc/now132.
[44] J. Zhao, et al., Immune and genomic correlates of response to anti-PD-1 immunotherapy in glioblastoma, Nat Med 25 (2019) 462–469, https://doi.org/10.1038/s41591-019-0349-y.
[45] B.A. Teicher, S.P. Fricker, CXCL12 (SDF-1)/CXCR4 pathway in cancer, Clin. Cancer Res. : an official journal of the American Association for Cancer Research 16 (2010) 2927–2931, https://doi.org/10.1158/1078-0432.CCR-09-2329.
[46] G.L. Gravina, et al., The novel CXCR4 antagonist, PRX177561, reduces tumor cell proliferation and accelerates cancer stem cell differentiation in glioblastoma preclinical models, Tumour biology : the journal of the International Society for Oncodevelopmental Biology and Medicine 39 (2017), 1010428317695528, https://doi.org/10.1177/1010428317695528.
[47] A. do Carmo, et al., CXCL12/CXCR4 promotes motility and proliferation of glioma cells, Cancer Biol. Ther. 9 (2010) 56–65, https://doi.org/10.4161/cbt.9.1.10342.
[48] I.T. Chiang, et al., Regorafenib reverses temozolomide-induced CXCL12/CXCR4 signaling and triggers apoptosis mechanism in glioblastoma, Neurotherapeutics : the journal of the American Society for Experimental NeuroTherapeutics 19 (2022) 616–634, https://doi.org/10.1007/s13311-022-01194-y.
[49] X. Sima, et al., Gene-gene interactions between interleukin-12A and interleukin-12B with the risk of brain tumor, DNA Cell Biol. 31 (2012) 219–223, https://doi.org/10.1089/dna.2011.1331.
[50] C.I. Cuzziol, M.M.U. Castanhole-Nunes, E.C. Pavarino, E.M. Goloni-Bertollo, MicroRNAs as regulators of VEGFA and NFE2L2 in cancer, Gene 759 (2020), 144994, https://doi.org/10.1016/j.gene.2020.144994.
[51] C. Luo, et al., LINC01564 promotes the TMZ resistance of glioma cells by upregulating NFE2L2 expression to inhibit ferroptosis, Mol. Neurobiol. 59 (2022) 3829–3844, https://doi.org/10.1007/s12035-022-02736-3.
[52] Q. Ju, et al., NFE2L2 is a potential prognostic biomarker and is correlated with immune infiltration in brain lower grade glioma: a pan-cancer analysis, Oxid. Med. Cell. Longev. (2020), 3580719, https://doi.org/10.1155/2020/3580719 (2020).
[53] F. Luan, et al., TNFRSF11B activates Wnt/beta-catenin signaling and promotes gastric cancer progression, Int. J. Biol. Sci. 16 (2020) 1956–1971, https://doi.org/10.7150/ijbs.43630.
[54] P. Luo, et al., Dysregulation of TMPRSS3 and TNFRSF11B correlates with tumorigenesis and poor prognosis in patients with breast cancer, Oncol. Rep. 37 (2017) 2057–2062, https://doi.org/10.3892/or.2017.5449.
[55] I.V. Kryvdiuk, et al., INHIBITION of IRE1 modifies effect of glucose deprivation on the expression of TNFalpha-RELATED genes in U87 glioma cells, Ukrainian Biochem. J. 87 (2015) 36–51, https://doi.org/10.15407/ubj87.06.036.
[56] S.H. Boots-Sprenger, et al., Significance of complete 1p/19q co-deletion, IDH1 mutation and MGMT promoter methylation in gliomas: use with caution, Mod. Pathol. : an official journal of the United States and Canadian Academy of Pathology, Inc 26 (2013) 922–929, https://doi.org/10.1038/modpathol.2012.166.
[57] A. Aibaidula, et al., Adult IDH wild-type lower-grade gliomas should be further stratified, Neuro Oncol. 19 (2017) 1327–1337, https://doi.org/10.1093/neuonc/nox078.
[58] E.K. Watson, et al., Personalised cancer follow-up: risk stratification, needs assessment or both? British journal of cancer 106 (2012) 1–5, https://doi.org/10.1038/bjc.2011.535.

[59] R.S. Riley, C.H. June, R. Langer, M.J. Mitchell, Delivery technologies for cancer immunotherapy, Nat. Rev. Drug Discov. 18 (2019) 175–196, https://doi.org/10.1038/s41573-018-0006-z.
[60] K.R. Spencer, et al., Biomarkers for immunotherapy: current developments and challenges, American Society of Clinical Oncology educational book. American Society of Clinical Oncology. Annual Meeting 35 (2016) e493–e503, https://doi.org/10.14694/EDBK_160766.
[61] J. van den Bulk, E.M. Verdegaal, N.F. de Miranda, Cancer immunotherapy: broadening the scope of targetable tumours, Open biology 8 (2018), https://doi.org/10.1098/rsob.180037.
[62] F.F. Hu, C.J. Liu, L.L. Liu, Q. Zhang, A.Y. Guo, Expression profile of immune checkpoint genes and their roles in predicting immunotherapy response, Briefings Bioinf. 22 (2021), https://doi.org/10.1093/bib/bbaa176.